PHYSICAL REVIEW B **81**, 195214 (2010)

Distinguishing between tunneling and injection regimes of ferromagnet/organic semiconductor/ferromagnet junctions

R. Lin, F. Wang, J. Rybicki, and M. Wohlgenannt*
Department of Physics and Astronomy, Optical Science and Technology Center, University of Iowa, Iowa City, Iowa 52242, USA

K. A. Hutchinson
Department of Electrical and Computer Engineering, Optical Science and Technology Center, University of Iowa, Iowa City, Iowa 52242, USA

(Received 19 January 2010; revised manuscript received 1 April 2010; published 24 May 2010)

Magnetoresistance effects in organic semiconductor spin valves have recently been reported, and have been variously interpreted as being due to tunneling magnetoresistance or giant magnetoresistance. We introduce a criterion for distinguishing between tunneling and injection conductivity necessary for properly analyzing organic spin-valve phenomena. We measure current-voltage (*I-V*) characteristics in Co/AlO_x/rubrene/Fe junctions with a rubrene layer thickness, *d*, ranging from 5 to 50 nm. For $d \leq 10$ nm, the *I-V* traces are typical of tunnel junctions. At $d > 15$ nm, the tunneling current becomes negligibly small. At larger biases, however, a second type of conductivity sets in. In this regime, the *I-V* curves are strongly nonlinear and temperature dependent. By comparing these to *I-V* curves measured in organic light-emitting diodes, we assign the latter mode to injection into the organic layer followed by hopping transport. We observe a spin-valve effect only in the tunneling regime.

DOI: 10.1103/PhysRevB.81.195214 PACS number(s): 72.25.Hg, 72.25.Dc, 73.40.Mr, 75.47.De

I. INTRODUCTION

Spintronics deals with controlling and utilizing the electron spin degree of freedom through a variety of spin-dependent phenomena. The spin valve is the principal spintronic device and consists, in its most basic form, of two ferromagnetic electrodes separated by a nonmagnetic spacer layer. The two ferromagnetic electrodes are chosen to exhibit two distinct switching fields, and the device can be switched between a parallel and antiparallel magnetization configuration using an applied magnetic field, *B*. The significant difference in resistance between the two configurations is referred to as giant magnetoresistance (GMR). In GMR devices, typically metallic spacer layers are used, and the spin-polarized current is injected into and transported through the spacer layer. If a thin layer of insulator is chosen as the spacer layer instead of a metal, the corresponding effect is called tunneling magnetoresistance (TMR) (Refs. 1 and 2) because the spin-polarized carriers tunnel through the insulating layer. Utilizing semiconductors as spacer layers is particularly attractive because of the possibility of implementing spintronic logic devices. However, spin injection into semiconductors continues to be challenging, in part, because of the conductivity mismatch problem.[3] The search for new materials systems is therefore ongoing.

Recently, there has been increasing interest in using organic semiconductors for spintronics, motivated, in part, by their long spin-relaxation times.[4,5] The first demonstration of an organic spintronic device employed a planar structure of $La_{2/3}Sr_{1/3}MnO_3$ (LSMO) electrodes separated by an $\approx$100-nm-long channel of α-sexithiophene.[6] The first vertical organic spin-valve device, which utilized LSMO and Co as the ferromagnetic layers, was demonstrated by Xiong *et al.*[7] and exhibited a clear spin-valve effect. The relatively thick spacer layers employed in Ref. 7 (>100 nm) suggest that spin injection into the organic layer (rather than tunneling through it) must have occurred. However, these devices display a surprisingly low resistance at low bias (<100 mV), weakly temperature-dependent current-voltage (*I-V*) curves and approximately parabolic differential conductance traces. All of these properties are characteristic of tunneling, and are uncharacteristic of organic semiconductor devices that function by carrier injection and hopping transport [cf. organic light-emitting diodes (OLEDs) (Ref. 8)], as we will show below. Recently, TMR using the organic semiconductor rubrene was demonstrated with tunneling distances as long as 15 nm.[9]

Apparently both spin injection and spin tunneling are possible, and a criterion for a clear distinction between tunneling and injection is required for the proper analysis of spin-valve effects in organics. Since tunneling is expected to dominate in thin junctions but decays exponentially with increasing thickness,[10] there will be a critical thickness beyond which tunneling is improbable, and injection will become the dominant mode of conductivity. In our experiments, we looked for and identified this transition between the two modes of conductivity. A similar strategy was recently employed in LSMO/rubrene/Fe devices.[11]

The distinction between tunneling and spin injection is crucially important for possible semiconductor spintronics applications: only if the spin gets injected into the semiconductor (i.e., its wave function is entirely contained within the semiconductor) is the effective manipulation of its spin state, necessary for logic gates,[12,13] possible. We note that in inorganic semiconductor spintronics, identification of spin injection is possible using spin-orbit-coupling-based methods and Hanle effect measurements. In organic semiconductors, however, the minuteness of spin-orbit coupling[14] makes such measurements extremely difficult.[15] Furthermore, the very slow carrier drift velocity requires very small Hanle mag-

netic fields. The presence of hyperfine fields[16] will mask the Hanle effect. We note that two methods for detecting spin injection in organics have recently been demonstrated[17,18] using two-photon photoemission and low-energy muon-spin rotation, respectively. However, these are very complex experiments that are not widely available.

II. DEVICE FABRICATION AND MEASUREMENTS

Our devices were fabricated on Si wafers covered with 300 nm of thermal oxide. The wafers were diced into 12.5 $\times 9$ mm^2 pieces, washed in several solvents and finally cleaned in an oxygen plasma cleaner. All these steps were performed in a class 1000 clean room. A 15-nm-thick Co electrode was deposited by electron-beam evaporation through a shadow mask in high vacuum at a rate of 0.1 nm/s and covered by a 2.5-nm-thick Al layer, also deposited by e-beam evaporation. The Al layer was then oxidized *ex situ* in an oxygen plasma. The Al-layer thickness and plasma oxidation time were chosen to yield a maximum room-temperature TMR signal of $\approx 8-10$ % in a Co/Al oxide/Fe device. The purpose of the Al-oxide (AlO) layer is to crucially improve the film quality of the organic film that will be grown on top of it because we found, in agreement with earlier work,[9,19–21] that organics grow more uniformly and with a smoother surface on oxides than on metals. The rubrene spacer layer was grown by thermal evaporation in high vacuum at a rate of 0.1 nm/s. All fabrication steps involving the organic layer were performed inside a glovebox or inside the glovebox-integrated vacuum evaporation chamber. Finally, a 15-nm-thick Fe top electrode covered by 15 nm of Al was deposited by electron-beam evaporation at a rate of 0.1 nm/s. The rms roughness of the individual layers was measured using atomic force microscopy in unfinished devices as follows: Co: ≈ 300 pm and rubrene at 10 nm: ≈ 600 pm. 12 devices of an area of 130×130 μm^2 were fabricated on each substrate. The substrates were then mounted inside a closed-cycle He cryostat located between the poles of an electromagnet. *I-V* and MR measurements were performed using a Keithley 2400 source measure unit, with the positive pole connected to the Co electrode. The *I-V* curves reported here were typically obtained by measuring ≈ 5 devices on a substrate and averaging the corresponding data. This resulted in low noise traces that can be numerically differentiated resulting in differential conductance traces. The reported MR traces are for individual junctions.

For comparison, we also fabricated a rubrene device using electrode materials commonly employed for fabricating OLEDs, specifically poly(3,4-ethylenedioxythiophene) poly-(styrenesulfonate) (PEDOT) spin coated on top of an indium-tin-oxide-covered glass slide as the bottom electrode, and Ca covered by Al as the top electrode. Otherwise, the fabrication procedures for the rubrene OLED follow that of the ferromagnetic junctions described above. The device area was $\approx 750 \times 750$ μm^2 and the rubrene layer thickness was 20 nm.

Magneto-optic Kerr effect (MOKE) measurements were performed at various temperatures using a focused HeNe laser beam. Changes in beam polarization were detected by measuring the intensity reflected off the sample located between two crossed polarizers as a function of B. A Si detector and a lock-in amplifier (together with an optical chopper) were used for measuring the light intensity. The MOKE data for the bottom Co electrode was measured directly on the electrode line of the device whereas the MOKE data for the top Fe electrode was measured on an electrode line deposited on top of a 10 nm rubrene film. In the latter measurement, the Fe/rubrene interface is optically inaccessible and the Fe/air interface was measured instead.

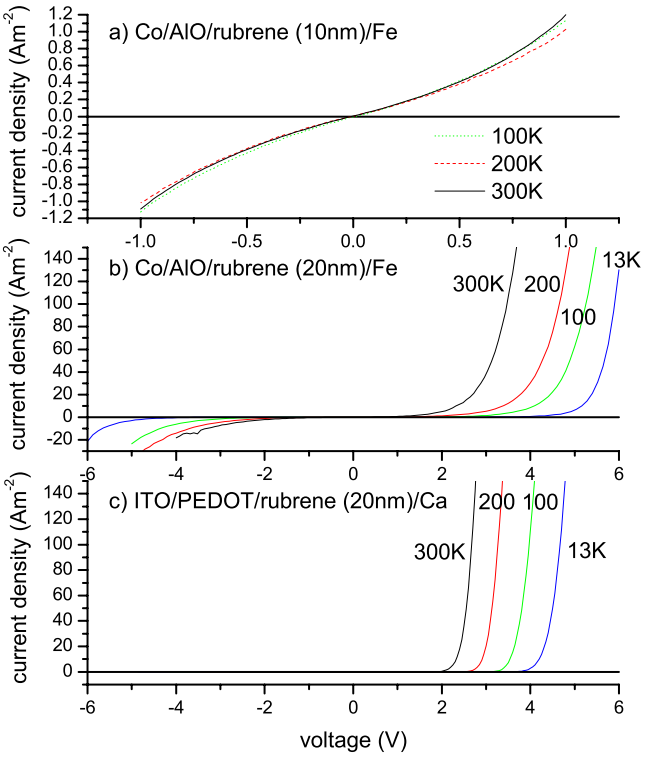

FIG. 1. (Color online) (a) and (b) Current-voltage (*I-V*) characteristics of Co/AlO/rubrene/Fe junctions at different temperatures. (a) Device with rubrene thickness of 10 nm. Note that the *I-V* curves for 100, 200, and 300 K are almost overlapping. (b) Device with rubrene thickness of 20 nm. (c) *I-V* characteristics of a PEDOT/rubrene (20 nm)/Ca OLED at different temperatures.

III. EXPERIMENTAL RESULTS AND DISCUSSION

A. Current-voltage characteristics

Figures 1(a) and 1(b) show measured *I-V* traces in devices with two different rubrene thicknesses, 10 nm and 20 nm, respectively, at various temperatures ranging from room temperature to ≈ 13 K. Figures 2(a) and 2(b) show room-temperature *I-V* data of devices with several different rubrene thicknesses, d, this time plotted as differential conductance versus the (average) electric field. The electric field was determined by dividing the voltage by the sum thickness of the AlO and rubrene films. We note that a typical resistance measured in our Co/AlO/Fe devices is less than 1 kΩ whereas the typical resistance in even our thinnest rubrene devices is on the order of 100 kΩ at compa-

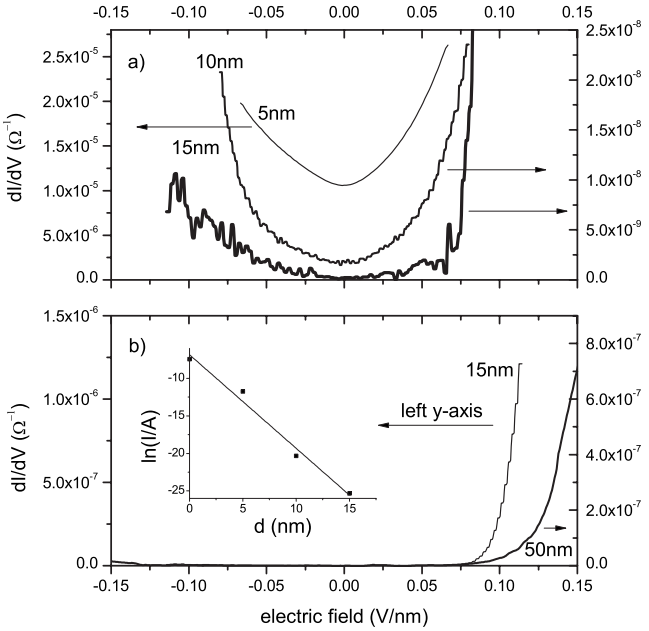

FIG. 2. Differential conductance versus average electric field of Co/AlO/rubrene/Fe junctions at room temperatures for different rubrene thicknesses, d. (a) $d=5$, 10, and 15 nm. (b) $d=15$ and 20 nm. Notice that the data in both panels are plotted on two different y scales, left and right y axis. The corresponding y axis is assigned using an arrow. Inset: natural logarithm of the tunneling current I measured in A at a bias voltage of 0.5 V versus d. The 0 nm data refers to a Co/AlO/Fe junction. The line is a fit to an exponential.

rable bias suggesting that our rubrene layers are near-pinhole free. Comparison of the data shown in Figs. 1(a) and 2(a) with that shown in Figs. 1(b) and 2(b) makes it clear that there exist two entirely different modes of conductivity in our devices. The mode shown in Figs. 1(a) and 2(a) displays weak temperature dependence and near-parabolic differential conductance traces typical of tunneling conduction and occurs in devices with thickness $d \leq 15$ nm. Our data agrees with data published for similar TMR devices with similar thicknesses by the MIT group.[9] The tunneling nature of this mode is confirmed by plotting the junction current measured at a bias voltage of 0.5 V vs d. As expected for tunneling, the dependence is exponential, from a fit to the dependence $\ln(I) \propto -d/d_0$ we obtain a tunneling decay length, $d_0 \approx 1$ nm, i.e., the length at which the conductivity has dropped to $1/e$ times the value of the Co/AlO/Fe "0 nm" device (to avoid confusion, we emphasize that d is the thickness of the rubrene layer alone, not including the AlO layer).

The mode shown in Figs. 1(b) and 2(b), on the contrary, is strongly temperature dependent, and the I-V curves are typical of those commonly measured in OLEDs. They possess an onset voltage below which hardly any current flows, and above which the current increases in a highly nonlinear fashion. The similarity to OLEDs is clearly demonstrated by comparison with Fig. 1(c) which depicts data measured in a rubrene OLED. Both Figs. 1(b) and 1(c) show a very similar functional dependence between current and voltage, as well as a characteristic temperature dependence where, with decreasing temperature, larger and larger biases are required to obtain a certain conductivity. Since current conduction in OLEDs is well known to occur by carrier injection followed by carrier hopping,[22] we assign the second mode observed in our ferromagnet/organic semiconductor/ferromagnet junctions to carrier injection/hopping.

OLED I-V curves are commonly explained by either a space-charge-limited current model[22] or modeled by Monte Carlo simulations considering (nearest neighbor) hopping in a disordered density of states.[23] In both models, the high nonlinearity is caused by a distribution of deep traps. Figure 2(a) shows that the tunneling current is barely detectable for the 15 nm device (note that the data are plotted on two different y scales, left and right y axis), and shows the beginning of the injection mode at a bias of ≈ 75 mV/nm. The 15 nm data is replotted in Fig. 2(b) on a larger y scale to demonstrate the dominance and high nonlinearity of the injection mode at larger biases. Figure 2(b) also shows the differential conductance of a much thicker device ($d=50$ nm) demonstrating injecting behavior.

In a recent work, Yoo *et al.*[11] performed a study of LSMO/rubrene/Fe junctions. They identified two modes of conductivity: tunneling and a mode they called phonon-assisted field emission. In the latter mode, carriers are injected into the organic layer even at low bias, resulting in I-V curves that look similar to the tunneling case. This mode of injection is different from the injection mode we found in this work, for which the conductivity at low bias is negligible. Injection due to field emission at low bias can occur only as a temperature-activated process because the carriers must overcome a significant energy offset between electrode work function and unoccupied energy levels in the organic. As a result, this injection mode is highly temperature dependent but even at room temperature, the electrode injection resistance is quite large and the device conductivity is injection limited. We do not observe this mode in our experiments, where the I-V curves exhibit a direct transition from tunneling to OLED-like, i.e., bulk-limited hopping conductivity (see Sec. III C). Schoonus *et al.*[24] recently observed a transition from singlestep to multistep tunneling in CoFeB/Al_2O_3/tris (hydroxyquinoline)aluminum (Alq_3)/Co spin valves as the Alq_3 layer thickness increases from 1 nm to 4 nm.

B. Magnetoresistance

Figure 3 shows magnetoconductivity traces, $\Delta I/I \equiv \frac{I(B)-I(B_{max})}{I(B_{max})}$ measured in two devices, one with $d=5$ nm (thin lines) and the other with $d=10$ nm (thick lines) at two different temperatures, 300 K and 100 K [panels (a) and (b), respectively]. B_{max} is the maximum reported field in the respective graphs, and corresponds to a parallel orientation of the two electrodes. At 100 K, both devices show a maximum MR ratio of 5–6 % which shows that spin-polarized tunneling can occur over lengths ≥ 10 nm. Our observation is consistent with results obtained by the MIT group for rubrene.[9] For the 10 nm device, a similar MR ratio is also achieved at room temperature whereas the MR ratio for the 5 nm device is significantly smaller than its 100 K value. This possibly indicates a competing pin-hole transport mechanism active at room temperature in the very thin junction. We note that we

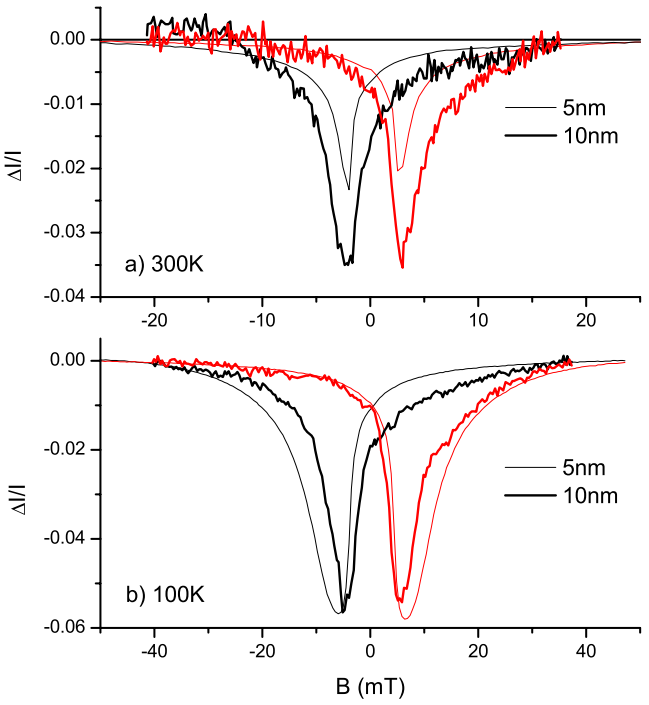

FIG. 3. (Color online) Magnetoconductivity traces measured at a bias of 0.2 V in a Co/AlO/rubrene (5 nm)/Fe device (thin lines) and a Co/AlO/rubrene (10 nm)/Fe device (thick lines), at room temperature [panel (a)] and 100 K [panel (b)].

found a device to device variation of ≈1% absolute in MR but somewhat larger than that for the 5 nm devices at room temperature. The figures also demonstrate that the coercive field of the electrodes increases significantly with decreasing temperature. Such behavior was also previously observed in organic spin valves[7] and may indicate pinning of domains on the organic semiconductor surface.

Figure 4 shows a comparison between the magnetoconductivity data for the 10 nm rubrene device and MOKE data for the ferromagnetic electrodes. The comparison is shown for room temperature in panel (a) and for 100 K in panel (b). The MOKE data for the bottom Co electrode was measured directly on the electrode line of the device and reproduces the switching behavior of the lower electrode observed in the magnetoconductivity data quite well. The top Fe electrode interface with rubrene is however optically inaccessible because the Si substrate is opaque at the HeNe laser wavelength. Instead, a Fe electrode line was deposited on top of a rubrene-covered Si substrate, and the MOKE data was measured for the Fe-air interface. Although the MOKE data for the Fe electrode agrees reasonably well with the magnetoconductivity data, and accurately reproduces the temperature dependence of the switching field, the MOKE data exhibits a much sharper switching behavior than that observed in the magnetoconductivity data. This discrepancy may be due to the fact, as described above, that we cannot measure the rubrene/Fe interface directly. At present, we do not have a firm explanation for the rather rounded switching of the top Fe electrode observed in the magnetoconductivity data but it could be due to imperfections in the rubrene/Fe interface. We will address this issue in our future work.

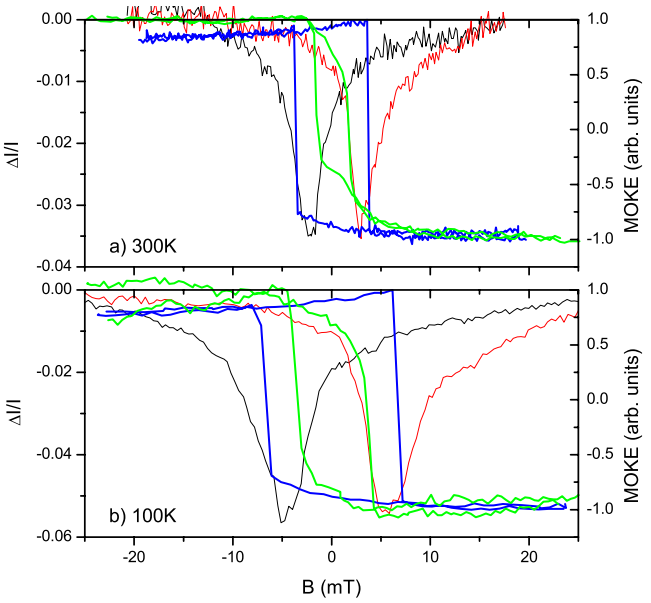

FIG. 4. (Color online) Comparison between magnetoconductivity traces measured at a bias of 0.2 V in a Co/AlO/rubrene (10 nm)/Fe device (thin lines) and magneto-optic Kerr effect traces (thick lines), at room temperature [panel (a)] and 100 K [panel (b)]. For the MOKE data, the inner loop is for the Co bottom electrode and the outer loop for the Fe top electrode.

For the 15 nm device, the tunneling current has become very small even at larger biases [see Fig. 2(a)], and no MR (with roughly 0.1% accuracy) could be detected. We have similarly been unable to detect any MR for thicker devices (at the necessarily larger biases required for measurable conductivity). The absence of TMR at these larger biases is not unexpected since we found, in agreement with other works on tunneling junctions,[9] that the MR ratio decreases significantly with increasing bias voltage. In addition, no MR was detected at biases leading to injection conductivity.

C. Discussion

Our results yield a value of ≈1 nm for the tunnel decay length in rubrene (see Fig. 2, inset). A measurable tunneling conductivity through the organic semiconductor layer is limited to devices of ≈15 nm thickness or thinner. Reports of GMR effects in organic spin valves with a thickness in excess of 100 nm (Refs. 7, 25, and 26) clearly seem beyond the tunneling range. Tunneling scenarios in such thick devices would only be plausible if there existed locally thin regions in the organic layer (i.e., the film quality is poor or effects occurring at sharp edges of devices) or if the effective barrier height for tunneling through the organic were exceptionally low. The latter scenario is highly unlikely, because d_0 is proportional to the square root of the barrier height, and a tenfold larger d_0 would require a tunnel barrier 100-fold smaller than in our devices.

If one rejects tunneling through the thick organic layer as a possibility for the spin valves reported in Refs. 7, 25, and 26, then an alternate explanation is required for their *I-V* curves which are clearly characteristic of tunneling, and not

injection, devices. This is possible modeling the devices as a series of (at least) two resistors. One corresponds to the resistance to carrier injection from the electrodes into the organic. Another represents the resistance to the transport of the carrier/spin through the organic. In OLEDs, efficient hole- and electron-injection electrodes are employed (such as PEDOT and Ca, as in the case of the OLED data we report here) resulting in small injection resistance and bulk-limited devices. However, in devices using LSMO, Co, or Fe, the injection resistance will be much larger than in OLEDs since these materials are much less efficient injectors due to their unfavorable work functions. Assuming that the devices in Refs. 7, 25, and 26 are (tunneling) injection limited rather than bulk limited, their *I-V* curves would mimic tunneling even though carriers get injected into the organic.

Such a scenario could also explain the recent observation of injection GMR in LSMO/rubrene/Fe junctions in the regime of phonon-assisted field emission.[11] In these devices, conduction is still injection limited. Because the spin-dependent injection resistance is much greater than the spin-independent bulk resistance, the possible conductivity mismatch problem is overcome.[27,28] We note however that we did not observe this scenario in our study using Co and Fe as the electrode materials. For thin devices, we observed tunneling through the devices, as evidenced by the exponential decay of the current with increasing layer thickness. In our devices with $d \geq 15$ nm, however, the *I-V* curves are like those of typical OLEDs and therefore typical of bulk-limited devices. In bulk-limited devices, the resistance of the organic semiconductor outweighs the injection resistance, and the conductivity mismatch may apply. This could explain the absence of injection GMR in our devices. We note that whereas the conductivity mismatch problem is well established for inorganic semiconductor spintronics, the situation is much less understood in organic spintronics. Nevertheless, significant progress in the modeling of organic spintronics devices has been made (Refs. 5, 29, and 30, and references therein). Schoonus *et al.*[24] recently demonstrated a loss of spin-valve signal as the mode of conductivity changes from singlestep to multistep tunneling in $CoFeB/Al_2O_3Alq_3/Co$ devices. This shows that additional mechanisms of loss of spin-polarization are active once spins get injected into the organic and may provide another reason for the absence of spin-valve signal in the injection devices we studied.

IV. SUMMARY

We have clearly demonstrated two different modes of conductivity in Co/AlO/rubrene/Fe junctions. The first mode, tunneling, occurs in relatively thin junctions, $d < 15$ nm, and decays exponentially with increasing rubrene thickness. We determined the tunneling decay length to be ≈ 1 nm. The tunneling mode is also characterized by a weak temperature dependence and a nearly parabolic differential conductance. The second mode, injection followed by hopping, occurs in relatively thick devices, $d \geq 15$ nm, and can be identified by strongly temperature dependent, highly nonlinear *I-V* traces that are similar to those commonly measured in OLEDs. We observed magnetoresistance in devices with a rubrene thickness of 5 and 10 nm. Those devices are clearly in the tunneling regime. For the 15 nm device, for which the tunneling current is just barely measurable we could not observe magnetoresistance. Giant magnetoresistance could also not be detected in the injection regime (for $d \geq 15$ nm). The conductivity mismatch problem provides a possible explanation for the absence of magnetorsistance in this regime. Carefully distinguishing between tunneling and injection is important for properly analyzing spin-valve phenomena in organic semiconductor devices, in particular, for proving spin injection.

ACKNOWLEDGMENTS

This work was supported by Army MURI under Grant No. W911NF-08-1-0317 and NSF under Grant No. ECS 07-25280.

*markus-wohlgenannt@uiowa.edu

[1] M. Julliere, Phys. Lett. A **54**, 225 (1975).
[2] J. S. Moodera, L. R. Kinder, T. M. Wong, and R. Meservey, Phys. Rev. Lett. **74**, 3273 (1995).
[3] G. Schmidt, D. Ferrand, L. W. Molenkamp, A. T. Filip, and B. J. van Wees, Phys. Rev. B **62**, R4790 (2000).
[4] W. J. M. Naber, S. Faez, and W. G. van der Wiel, J. Phys. D **40**, R205 (2007).
[5] V. A. Dediu, L. E. Hueso, I. Bergenti, and C. Taliani, Nat. Mater. **8**, 707 (2009).
[6] V. Dediu, M. Murgia, F. C. Matacotta, C. Taliani, and S. Barbanera, Solid State Commun. **122**, 181 (2002).
[7] Z. H. Xiong, D. Wu, Z. V. Vardeny, and J. Shi, Nature (London) **427**, 821 (2004).
[8] P. E. Burrows and S. R. Forrest, Appl. Phys. Lett. **64**, 2285 (1994).
[9] J. H. Shim, K. V. Raman, Y. J. Park, T. S. Santos, G. X. Miao, B. Satpati, and J. S. Moodera, Phys. Rev. Lett. **100**, 226603 (2008).
[10] W. H. Butler, X. G. Zhang, T. C. Schulthess, and J. M. MacLaren, Phys. Rev. B **63**, 054416 (2001).
[11] J. W. Yoo, H. W. Jang, V. N. Prigodin, C. Kao, C. B. Eom, and A. J. Epstein, Phys. Rev. B **80**, 205207 (2009).
[12] S. Datta and B. Das, Appl. Phys. Lett. **56**, 665 (1990).
[13] R. Fiederling, M. Keim, G. Reuscher, W. Ossau, G. Schmidt, A. Waag, and L. W. Molenkamp, Nature (London) **402**, 787 (1999).
[14] J. Rybicki and M. Wohlgenannt, Phys. Rev. B **79**, 153202 (2009).
[15] Z. V. Vardeny, Nat. Mater. **8**, 91 (2009).
[16] P. A. Bobbert, W. Wagemans, F. W. A. van Oost, B. Koopmans, and M. Wohlgenannt, Phys. Rev. Lett. **102**, 156604 (2009).
[17] M. Cinchetti, K. Heimer, J. P. Wustenberg, O. Andreyev, M. Bauer, S. Lach, C. Ziegler, Y. L. Gao, and M. Aeschlimann, Nat. Mater. **8**, 115 (2009).

[18] A. J. Drew, J. Hoppler, L. Schulz, F. L. Pratt, P. Desai, P. Shakya, T. Kreouzis, W. P. Gillin, A. Suter, N. A. Morley, V. K. Malik, A. Dubroka, K. W. Kim, H. Bouyanfif, F. Bourqui, C. Bernhard, R. Scheuermann, G. J. Nieuwenhuys, T. Prokscha, and E. Morenzoni, Nat. Mater. **8**, 109 (2009).

[19] K. V. Raman, S. M. Watson, J. H. Shim, J. A. Borchers, J. Chang, and J. S. Moodera, Phys. Rev. B **80**, 195212 (2009).

[20] B. Nickel, in *Physical and Chemical Aspects of Organic Electronics*, edited by C. Woll (Wiley-VCH, Weinheim, 2009), pp. 301–315.

[21] T. S. Santos, J. S. Lee, P. Migdal, I. C. Lekshmi, B. Satpati, and J. S. Moodera, Phys. Rev. Lett. **98**, 016601 (2007).

[22] P. W. M. Blom and M. Vissenberg, Mater. Sci. Eng., R. **27**, 53 (2000).

[23] H. Bässler, Phys. Status Solidi B **175**, 15 (1993).

[24] J. J. H. M. Schoonus *et al.*, Phys. Rev. Lett. **103**, 146601 (2009).

[25] V. Dediu, L. E. Hueso, I. Bergenti, A. Riminucci, F. Borgatti, P. Graziosi, C. Newby, F. Casoli, M. P. De Jong, C. Taliani, and Y. Zhan, Phys. Rev. B **78**, 115203 (2008).

[26] Y. Liu, S. M. Watson, T. Lee, J. M. Gorham, H. E. Katz, J. A. Borchers, H. D. Fairbrother, and D. H. Reich, Phys. Rev. B **79**, 075312 (2009).

[27] E. I. Rashba, Phys. Rev. B **62**, R16267 (2000).

[28] A. Fert and H. Jaffres, Phys. Rev. B **64**, 184420 (2001).

[29] P. P. Ruden and D. L. Smith, J. Appl. Phys. **95**, 4898 (2004).

[30] J. F. Ren, J. Y. Fu, D. S. Liu, L. M. Mei, and S. J. Xie, J. Phys.: Condens. Matter **17**, 2341 (2005).